Particle
& Particle Systems Characterization
www.particle-journal.com

Versatile Graphene Quantum Dots with Tunable Nitrogen Doping

Yunqian Dai, Huan Long, Xiaotian Wang, Yueming Wang, Qing Gu, Wei Jiang, Youcheng Wang, Cancan Li, Tingying Helen Zeng, Yueming Sun, and Jie Zeng**

This paper reports a facile fabrication of N-doped graphene quantum dots (N-GQDs) showing controllable chemical properties through a hydrothermal treatment. The N-GQDs have a uniform size of 3.06 ± 0.78 nm and prefer the equilibrium shapes of circle and ellipse due to the minimization of edge free energy. The *N/C* atomic ratio in N-GQDs can be precisely tailored in a range from 8.3 at% to 15.8 at% by simply controlling the concentration of N source (ammonium hydroxide). One order of magnitude quantum yield of 34.5% is achieved by N-GQDs, compared with the N-free GQDs, as the substitutional N has an essential role in more effective radiative emission. Excessive N dopants in N-GQDs can lead to photoluminescence quenching, through non-radiative transition back to the ground state. The N-GQDs are further found to be suitable as photocurrent conversion materials due to benign energy matching with anatase nanofibers, the ultrafast electron injection at their interface, and efficient electron transfer. This work provides an efficient and inspiring approach to engineering both chemical components and physical properties of N-GQDs, and will therefore promote their basic research and applications in energy conversion.

1. Introduction

The ideal 2D graphene sheet, which consists of sp^2-hybridized carbon atoms, is widely known as zero-bandgap semiconductor.[1] Engineering intrinsic, chemical, and/or physical properties of 2D graphene structures are believed to have promising applications in nanotechnologies.[2–4] Among various viable methods, reducing the size down to ~10 nm provides an effective way to manipulate their band structural, optical, electronic, magnetic, and electrochemical features due to quantum confinement and edge effect.[5–8] One typical achievement of this strategy is the graphene quantum dots (GQDs) with a size less than 20 nm,[9–12] which is mainly composed by several hundred to thousand conjugated carbon atoms.[13] Apart from the geometrical engineering, recent progress in doping graphene with heteroatoms, such as electron-rich nitrogen (N), has also proved potent manipulation of local chemical features and bandgaps of 2D graphene structures, enabling p-type or n-type conductivity.[14]

As a fruit of these two methods, the N-doped GQD (denoted as N-GQD) has only recently emerged, although it has attracted extensive research interests. Recent efforts on N-GQDs demonstrated its excellent electrocatalytic activities for oxygen reduction reaction (ORR) even comparable with noble metals, although they have a low *N/C* atomic ratio of only 4.28 at% by electrochemical or solution-phase fabrication.[15,16] Besides, owing to N-doping or amino-group functionalization, optical properties of GQDs significantly changed, including the emergence of upconversion photoluminescence (PL) associated with nanosecond-long PL lifetime.[17,18] Despite these developments, N dopants in the π-conjugated framework are still far from controllable in terms of their distributions and bonding configurations: their concentration is typically less than 5 at% and their locations are only pyridinic sites or sometimes observed pyrrolic sites.[15–18] However, substitutional N-doping is more seductive than the interstitial counterpart, which can vastly tailor the band structure of graphene and possibly make for unique properties.[1] But such doping is still challenging to be realized in graphene through a solution-phase approach. As a result, the substitutional N-GQDs have been rarely observed. In this regard, this paper presents a facile method to the synthesis of substitutional N-GQDs, which are controllable both in dopant concentration and bonding configuration, inspiring maneuvering of their intrinsic features particularly with respect to luminescence and semiconducting properties.

Dr. Y. Dai, H. Long, X. Wang, Y. Wang, Q. Gu,
Prof. W. Jiang, C. Li, Prof. Y. Sun
School of Chemistry and Chemical Engineering
Southeast University
Nanjing, Jiangsu, 211189, PR China
E-mail: daiy@seu.edu.cn
Y. Wang, Prof. J. Zeng
Hefei National Laboratory for Physical Sciences at the Microscale
University of Science and Technology of China
Hefei, Anhui, 230026, PR China
E-mail: zengj@ustc.edu.cn
Dr. T. H. Zeng
Center for Excitonics
Research Laboratory for Electronics
Massachusetts Institute of Technology
Cambridge, MA, 02139, USA

DOI: 10.1002/ppsc.201300268

2. Experimental Section

N-Doping of Graphene Quantum Dots (N-GQDs): Graphene oxide (GO) colloids were prepared according to our previous report and acted as the starting carbon materials.[19] 20 mg of GOs colloid was first diluted with ammonium hydroxide (NH_4OH, 28–30 wt%; Sigma), and the total volume was adjusted by Millipore water to 20 mL to obtain 1.9 mol L^{-1} or other indicated concentrations. This yellow–brown colloid was mildly ultrasonicated for several minutes to ensure its homogeneity, then carefully transferred into a Teflon-line stainless-steel autoclave. Nitrogen doping was performed via hydrothermal treatment at 200 °C for 8 h. After cooling down to room temperature, the desired N-GQDs at the supernatant were centrifuged at 15 000 rpm for 30 min, therefore trace amount of brown–black unsoluble fragments was carefully removed. Finally, the supernatant was dried by a rotating evaporator then redispersed in Millipore water for dialyzing in a tubing bag (Molecular weight cut off = 3500 Da) for one day.

Quantum Yields (QYs) Measurement: The QYs of quantum dots were determined by using RhB as the standard sample, and were calculated according to the following equation:

$$\Phi = \Phi_r (I/I_r)(n^2/n_r^2)(A_r/A) \quad (1)$$

where Φ is the quantum yield, I is the measured integrated emission intensity, n is the refractive index, and A is the optical density. The subscript r refers to the standard (0.31 for RhB).[20]

Photoelectrochemical Response of N-GQDs: The dialyzed N-GQDs were dried then redispersed in 20 mL of ethanol. They were then mixed with 5 mg of electrospun anatase nanofibers according to previous reports[19,21,22] at room temperature and stirred in dark for 2 h. 20 µL of N-GQDs/TiO_2 was drop-casted on cleaned florin-doped tin oxide (FTO) glass with an active area of 0.25 cm^2, acting as both a working electrode and a photoanode. The three-electrode system was assembled by connecting the working electrode with a platinum wire as the counter electrode and the Ag/AgCl as the reference electrode. An aqueous solution of $NaNO_3$ (10×10^{-3} M) was used as the supporting electrolyte. The photoanode was irradiated by a 6 W UV lamp with a wavelength of 365 nm or Xenon lamp (with 420 nm cutoff filter, 241 mW). The photocurrent was recorded with CHI 760B electrochemical workstation (CH Instrument; Chenhua Co., Shanghai, China).

Characterizations: The high-purity N-GQDs were dropped on an ultrathin carbon film supported on holey copper grid observed under transmission electron microscope (TEM) using a Tecnai G2 T20 (FEI) operated at 200 kV. Energy-dispersive X-ray (EDX) analysis was performed on the EDX system attached to the same microscope. X-ray photoelectron spectroscope (XPS) measurements were performed with a Thermo Scientific K-Alpha using monochromatic Al Kα radiation. Fourier transform infrared (FTIR) spectra were recorded on a Thermo Nicolet 5700 spectrometer. UV–vis spectra were recorded on Shimadzu UV-2450 spectrophotometer and PL spectra were measured on Horiba Jobin Yvon FluoroMax-4 spectrofluorometer. The transient PL measurements were recorded at 413 nm with a 320 nm excitation on FLS900 Edinburgh Analytical Instruments at room temperature. Raman spectra were tested using Thermo Fisher Scientific DXR Raman Microscope with a 532-nm laser beam. The height profiles of N-GQDs and GOs were collected by atomic force microscope (AFM, Veeco) in tapping mode.

3. Results and Discussion

Based on our previous work, graphene oxides (GOs) with one to three layers were prepared and chosen as starting materials (Figure S1a, Supporting Information),[19] which then hydrothermally reacted in 1.9 mol L^{-1} of aqueous ammonium hydroxide (NH_4OH) at 200 °C. As shown in **Figure 1**a–c, the products—i.e., tiny N-GQDs—exhibited excellent uniformity with an average size of 3.06 ± 0.78 nm and are much smaller than their N-free counterpart GQDs (~10 nm).[23] The height profiles shown in Figure S1b,c (Supporting Information) confirmed their thickness of 0.67 ± 0.12 nm having one to two layers.[23] And the N-GQDs maintained uniform size of ~3 nm with increasing NH_4OH (Figure S2, Supporting Information) concentrations therefore allowed us to explore their size-independent properties. As shown in Figure S3 (Supporting Information), the N-GQDs were highly soluble in varied common solvents, including tetrahydrofuran (THF), ethanol, acetone, and dimethylformamide (DMF) as well as water.

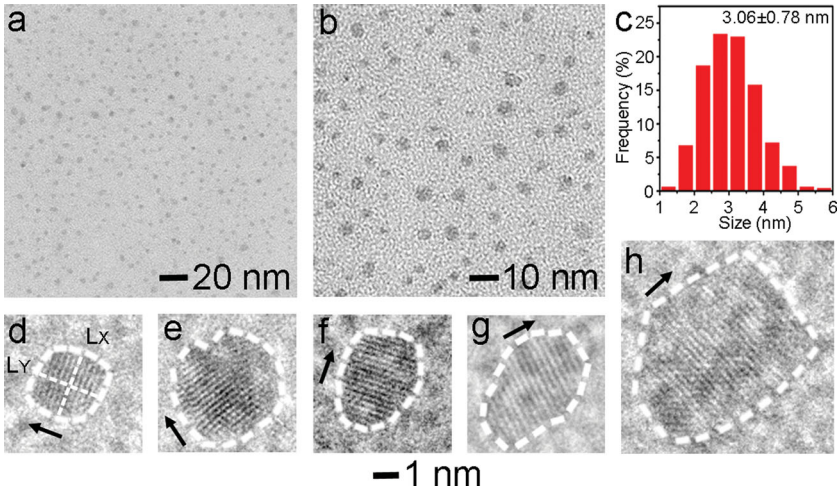

Figure 1. a,b) TEM images of N-doped graphene quantum dots (N-GQDs) hydrothermally fabricated in 1.9 mol L^{-1} of NH_4OH at 200 °C. c) The corresponding diagram of size distribution. HRTEM images of N-GQDs showing d,e) circular, f,g) elliptical, and h) less observed polygonal shapes. The black arrow indicates the <11$\bar{2}$0> direction for each case. In (d), L_X and L_Y are defined as the edges perpendicular and parallel to the <11$\bar{2}$0> directions, respectively.

Figure 1d–h shows high-resolution transmission electron microscopy (HRTEM) images of five N-GQDs with typical sizes and shapes, which showed good crystallinity with lattice distance of 2.42 Å, corresponding to the (11$\bar{2}$0) lattice fringes of graphene.[24] Short-dashed white curves were applied to outline the edges of each N-GQD. Most of the N-GQDs (ca. >80%) were regular in shape, such as circular (Figure 1d,e), elliptical (Figure 1f,g) and polygonal (Figure 1h), although a few of irregular shapes were also observed. The N-GQDs were further geometrically defined by the lateral lengths labeled L_X (perpendicular to <11$\bar{2}$0> direction) and L_Y (along with <11$\bar{2}$0> direction), respectively, and the L_Y/L_X value was estimated for simple comparison. 73% of N-GQDs had a L_Y/L_X value in the range of 1.0 ± 0.2, and showed circle or elliptical shapes (Figure 1d–g) consisting with curved peripheries.[25] Besides, polygonal shape was observed at a lower frequency (ca. ≈15%) and had a size bigger than 3 nm. On the contrary, such shape consisted with linear and partially curved peripheries. For example, the N-GQD in Figure 1h exhibited pentagonal shape with a L_Y/L_X of 1.3 and had a size of 6.24 nm (an average value of L_X and L_Y). Taken together, the N-GQDs preferred to form curved peripheries in thermodynamically equilibrium structures of circle

or ellipse to minimize edge free energies, through migration of uncombined C atoms, rearrangement of atoms (C, N, O, etc.), and/or reconstruction of crystallization.[26,27] The edge structures are the essential features of graphene, including zigzag- or armchair-edge configurations.[27] It is believed that the zigzag-edge appears at both the circle or straight periphery, while armchair-edge favorably appears at straight periphery in GQDs.[25] Therefore, it is reasonable to pose that the N-GQDs (Figure 1d–h) preferred zigzag-edges, in a pattern similar to the GQDs derived from carbon fibers.[24]

X-ray photoelectron spectroscopy (XPS) measurements were employed to uncover the chemical environmental changes induced by N dopants. As shown in Figure S4 (Supporting Information), a pronounced new signal appeared at ≈400 eV belongs to N 1s in N-GQDs, in addition to predominant C 1s and O 1s peak at ~285 eV and ~532 eV. The *N*/*C* atomic ratio was estimated to be as high as 14.0 at%, three times higher than those of N-GQDs prepared using ammonia gas or N-containing organics as the nitrogen sources, such as tetrabutylammonium perchlorate (TBAP) or acetonitrile. This result implies that the NH_4OH is a better nitrogen source for high concentration doping. It is worth noting that some functional groups in pristine GOs, such as O-rich groups in the form of carboxyl, epoxide, and hydroxyl groups were usually unexpectedly removed, owing to accelerated intramolecular and/or intermolecular dehydration in the superheated H_2O during hydrothermal reaction.[23,28] As demonstrated by Figure S4a (Supporting Information), the N-GQDs exhibited a high O/C atomic ratio of 58.6 at%, indicating O-rich groups were well restored. This is believed to be responsible for the observed exclusive PL features of GQDs and GO sheets in the following discussion.[15,29,30] The surface functional groups in the N-GQDs were also evidenced in Fourier transform infrared (FTIR) spectra (Figure S5, Supporting Information). Two new peaks assigned to the N–H in-plane and C–N in-plane stretching confirmed the successful introduction of large quantities of amine groups in N-GQDs. And the observation of sharp absorption bands of well-restored O-rich groups, e.g., C–OH and C–O, is consistent with the XPS measurements.

The N 1s high-resolution XPS spectrum in **Figure 2**a can be deconvoluted into signals for predominant pyrrolic N appearing at 399.7 eV (denoted as N1), trace amount of N-oxides at 403.1 eV (denoted as N2) and the N-containing (e.g., $–CONH_2$)[31] dangling bonds or physisorbed species at 406.9 eV (denoted as N3), all of which agree with previous assignment.[32] Previously reported N dopants in N-GQDs were mostly pyridinic with a peak at ~398.3 eV and a few pyrrolic N with a peak at ~399.6 eV.[18] The absence of pyridinic N here which appears at the edge of graphene plane can be ascribed to an ultra-high N dopant concentration.[31] Under this condition, N dopant tends to take the pyrrolic shape, bonded to two carbon atoms in the carbon lattice rather than the pyridinic shape, which is identical to that in N-doped graphene.[14]

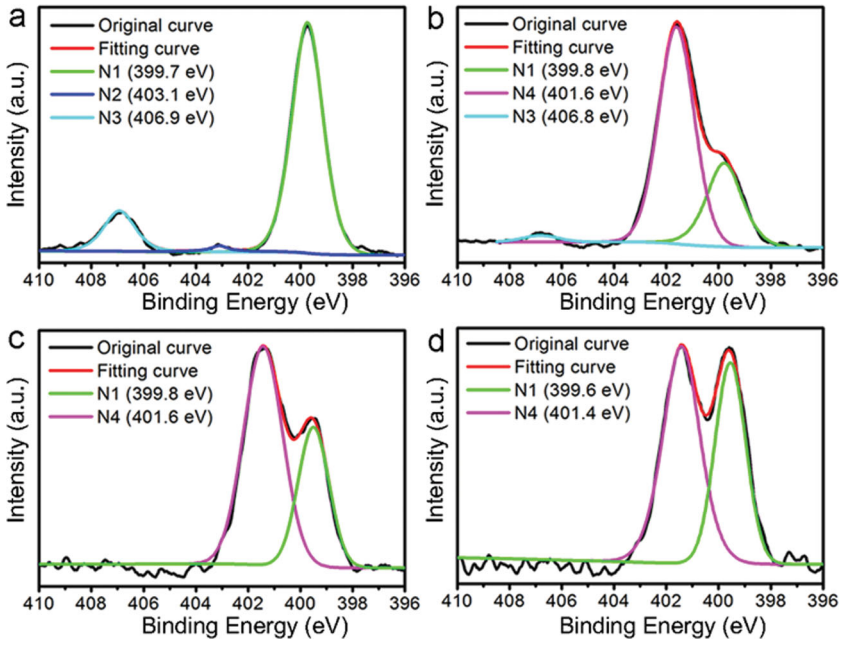

Figure 2. N *1s* high-resolution XPS spectra of the N-GQDs made in a) 1.9, b) 3.7, c) 5.6, and d) 7.4 mol L^{-1} of NH_4OH. N1: pyrrolic N; N2: N-oxides; N3: N-containing dangling bonds or physisorbed species; N4: substitutional N.

To control the doping ratio of N, we simply modulated the concentration of NH_4OH. As presented in **Table 1**, 3.7 mol L^{-1} of NH_4OH doubled the N source concentration and gave rise to an increase of *N*/*C* atomic ratio to 15.8 at%. The N-oxides disappeared and the N-containing dangling bonds also dramatically decreased. One possible reason is that an increased concentration of NH_4OH (with a low boiling point of 37.7 °C at 25 wt%) induced an increased high internal pressure in the hydrothermal reaction, which removed these less stable N atoms.[19] Strikingly, one new peak appeared at 401.6 eV (denoted as N4) (Figure 2b), which relates to the substitutional N rarely observed in previously reported N-GQDs.[15,16,18] The substitutional N, also called "graphitic nitrogen," refers to nitrogen atoms these replace carbon atoms within a graphene lattice.[1,31] Among the four N bonding types, substitutional is the only one that maintains the sp^2 hybridization of C atoms and can improve the electroconductivity in the graphene film by donating delocalized electrons.[32] As shown in Figure 2c, elevating the concentration of NH_4OH to 5.6 mol L^{-1} further increased the internal pressure and resulted in a slightly decreased *N*/*C* atomic ratio of 12.8 at%. The ratio eventually decreased to 8.3 at% in the concentration of 7.4 mol L^{-1} of NH_4OH (Figure 2d), but was still higher than that of reported N-GQDs.[15,18] For better comparison, the peak area ratios of substitutional N to pyrrolic N (*N*4/*N*1) were calculated to determine the atomic ratios of substitutional N to C (*N*4/*C*) and pyrrolic N to C (*N*1/*C*) (Table 1). The dependence of the atomic ratio of various N on the NH_4OH concentration was shown in Figure S6 (Supporting Information). The *N*1/*C* ratios kept almost constant, while the *N*4/*C* ratios were inverse proportional to the concentration of NH_4OH, once the NH_4OH reached a high concentration over

Table 1. Elemental analysis from XPS measurements as a function of NH_4OH concentration.

NH_4OH [mol L^{-1}]	*N*/*C* [at%]	*N*1/*C* [at%]	*N*4/*C* [at%]	*N*4/*N*1 peak area ratio
1.9	14.0	11.7	0	0.0
3.7	15.8	4.4	11.1	2.5
5.6	12.8	4.3	8.5	2.0
7.4	8.3	3.6	4.7	1.3

N1 and N4 are denoted as pyrrolic N and substitutional N, respectively.

3.7 M. That is, excessive NH_4OH in fact hampered the N doping by preventing the N bonding with substitutional sites, consequently diminishing the *N*/*C* atomic ratio, although such substitutional N is critical to the property of N-GQDs. Apparently, the doping of N into aromatic heterocycles is sensitive to their reaction condition particularly concerning, e.g., appropriate N source type and concentration during reaction.

The Raman spectra in **Figure 3** demonstrate the intrinsic characteristics of sp^2 carbon with disorder.[33] The typical features are the *D* band at ~1360 cm^{-1}, the *G* band at ~1580 cm^{-1}. Their intensity ratios expressed as I_D/I_G measures the disorder. The I_D/I_G of N-GQDs (e.g., in Figure 1) increased to ~1.10 from 0.96 for pristine GOs, although it was still smaller than that of N-free counterparts.[12] Following the empirical Tuinstra–Koening relation, the sp^2 cluster sizes (L_a) is proportional to $(I_D/I_G)^{-1}$,[34] while the distance between defects (L_d) is proportional to $(I_D/I_G)^{-1/2}$, on account of the presence of point-like defects in graphene.[14] Therefore, the N dopants as heteroatoms inevitably induced decreased L_a and L_d by disrupting the conjugated sp^2 cluster and accelerating point-like defect density through generating disordered structures.[35] But the defect density was controllably decreased at a lower *N*/*C* atomic ratio. For instance, the N-GQDs in Figure 2d exhibited an expectedly smaller I_D/I_G of 0.80, implying their relative high quality.[15] Their minor *D* band intensity was assigned to their

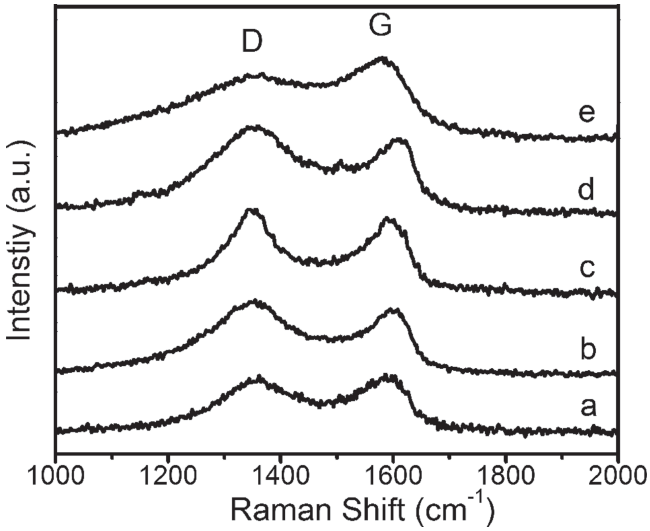

Figure 3. Raman spectra of a) pristine GOs and N-GQDs fabricated with b) 1.9, c) 3.7, d) 5.6, and e) 7.4 mol L^{-1} of NH_4OH.

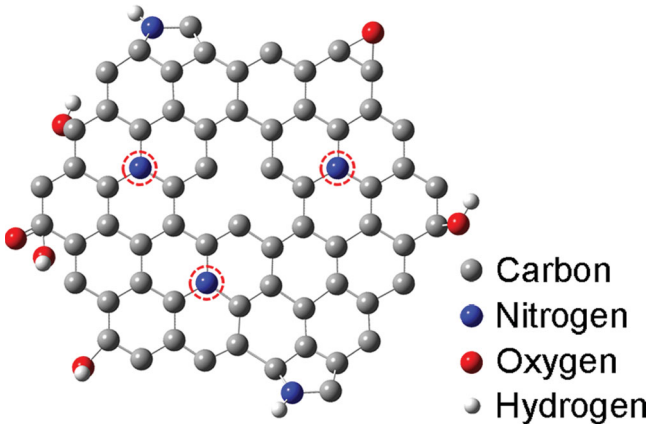

Scheme 1. Schematic illustration of the structure of the N-GQDs. The red, dash circles highlight three substitutional N atoms. To demonstrate the possible defect structure of the N-GQDs, one C atom is removed from the center of the model.

large amounts of edges,[36] while their down-shift G band was attributed to *n*-doping caused by in-plane substitution of N and its electronic effects.[37,38]

Taken together, in the N-GQDs, the sp^2-hybridized C atoms associated with graphitic N generate the sp^2 clusters in form of aromatic rings. The clusters are believed to be isolated in the neighboring sp^3-hybridized N/C/O matrix. As shown in **Scheme 1**, one possible structure of the N-GQDs was therefore proposed, in which three substitutional N dopants are marked by red dash circles.

Figure 4a shows the UV–vis absorption spectrum of the N-GQDs, indicating a broadened absorption shoulder at ca. 297 nm and a blue-shift of 23 nm compared to the GQDs. This absorption can be assigned to the π–π^* transition at aromatic sp^2 domains, and the blueshift is believed to originate from the strong electronic affinity of N dopants.[15,18] The π and π^* states that lies in the σ–σ^* gap mostly determined the optoelectronic features of carbon-based materials.[35,39] The inset in Figure 4a depicts the blue luminescence of N-GQDs under the irradiation of a 365 nm light. Note that, all four types of N-GQDs in Figure 2 which varied in *N*/*C* atomic ratio, in fact emitted similar intensive blue luminescence (Figure S7, Supporting Information), indicating they contained more or less similar sp^2 clusters in the sizes correlated to this energy gap.

The PL spectra excited with light of different wavelengths were analyzed to elucidate the mechanism. As shown in Figure 4b, the N-GQDs exhibited excitation-dependent PL emissions. As the excitation wavelength increased from 320 nm to 480 nm, the PL peaks starting at 413 nm accordingly redshifted as long as the gradual decrease in PL intensities, and had a Stokes-shift of 0.88 eV (93 nm). Several theoretic predictions of the relation of energy gap (E_g) versus size (*L*) for GQDs follows the equation as E_g (eV) = 1.68 eV nm/*L* on the basis of quantum confinement. And this equation was then experimentally calibrated to E_g (eV) = 1.77 ± 0.2 eV nm/$L^{0.9 \pm 0.1}$.[40] Therefore the bandgap of nanoscale GQDs cannot exceed ~1.0 eV.[41] Following this analysis, the N-GQDs in fact showed efficient high-energy PL emission whose wavelength corresponds to an energy gap even larger than the bandgap. However, due to

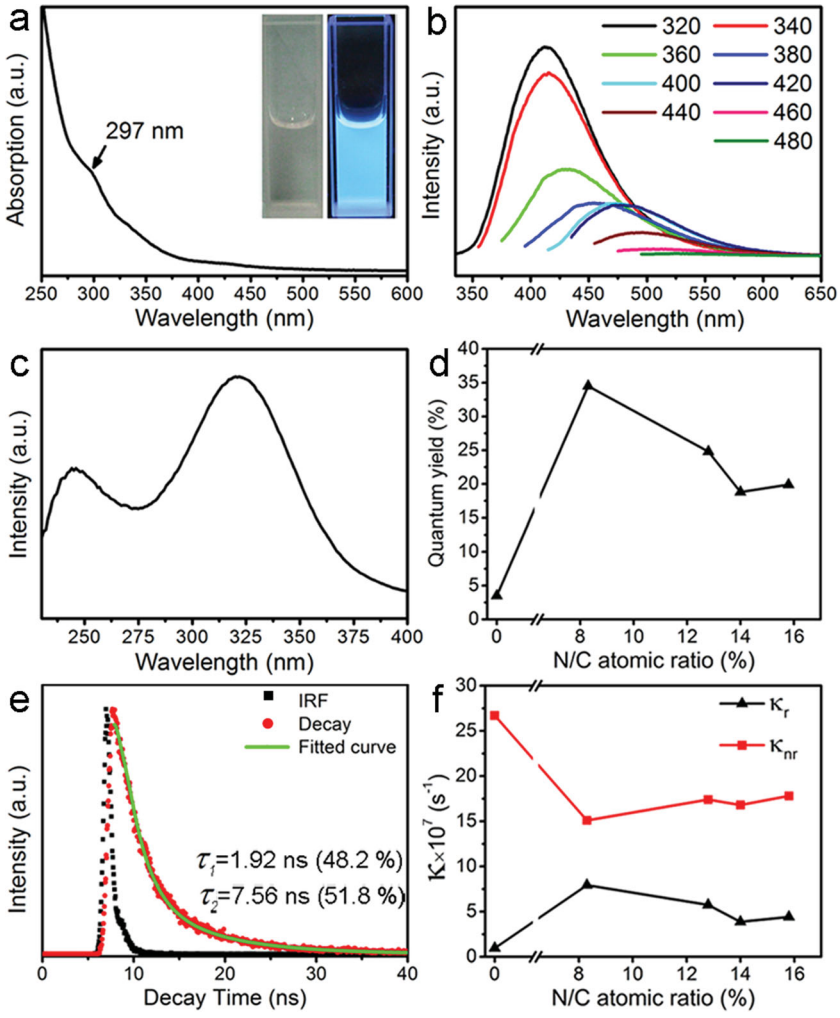

Figure 4. Optical properties of the N-GQDs. a) UV–vis spectrum, b) PL spectra emitted with the use of exciting lights with different wavelengths, and c) PLE spectrum with the detection wavelength at 413 nm. The N-GQDs were hydrothermally treated in 1.9 mol L^{-1} of NH_4OH. Insets in (a) are the photographs of the N-GQDs under visible (left) and 365 nm UV light (right) irradiation. d) The dependence of quantum yield for N-GQDs on the *N*/*C* atomic ratio. e) The transient PL measurements of N-GQDs in (a) record at room temperature. The insets show the lifetime data fitted by two-exponential function. f) A plot showing the dependence of the radiative rate constant (κ_r) and nonradiative rate constant (κ_{nr}) on the *N*/*C* atomic ratio.

quantum confinement effect, the energy gaps are determined mostly by the sp^2 cluster size. The wide size range of the sp^2 cluster sizes induced their wide energy gap region, normally from 2.25 eV (550 nm) to 3.00 eV (413 nm).[29] Consequently, the bandgap structure exhibits less signature feature responsible for the observed PL energy gap, and N-GQDs could show excitation-dependent PL emission.[28] Another possible explanation is grounded on the unique scattering mechanism for graphene, such as fast carrier–carrier scattering dominating over electron-photon scattering. As a result, the graphene also exhibited visible PL due to the minimization of thermalization or formation of excited-state relaxation channel, although it had no bandgap.[25,41] Like GQDs, N-GQDs emitted almost quenched PL in an acid aqueous (e.g., aqueous HCl, pH 1), while much stronger PL in alkaline aqueous (e.g., in NaOH aqueous, pH 13) (Figure S8, Supporting Information), implying emissive zigzag-edges sites were the origin of PL emission.[12] No detectable shift of PL peak was observed, as no change occurred in correlated sp^2 cluster sizes. The zigzag-edges sites and sp^2 cluster sizes may independently affect the PL peak intensity and profile.

We performed the PL excitation (PLE) spectroscopy to investigate the recombination process of electron-hole (e^--h^+) pairs responsible for the PL emission (Figure 4c and Figure S9a, Supporting Information). Two distinct peaks at 5.06 eV (245 nm) and 3.88 eV (320 nm) can be regarded as the two types of the electron transitions from σ and π orbitals in highest occupied molecular orbitals (HOMOs), to the lowest unoccupied molecular orbitals (LUMOs). This electronic transition is depicted in Figure S9 (Supporting Information). Therefore, the energy difference (δE) between the σ and π orbitals was determined to 1.16 eV. This experimental finding is consistent with the PL emission mechanism, which originated from the emissive zigzag-edge sites with a carbene-like triplet $\sigma^1\pi^1$ ground state.[10,16,30,35] Variety in N dopants slightly modulated the δE between the σ and π orbitals Figure S9 (Supporting Information).

The quantum yields (ϕ) of N-GQDs under various circumstances are generalized in Table S1 (Supporting Information). Compared with a low quantum yield (3.50%) observed in N-free GQDs, all N-GQDs exhibited dramatically increased quantum yields. For instance, the present N-GQDs in Figure 2a exhibited a significantly increased quantum yield of 18.8%, and quantum yield was improved to 34.1% by simply redispersing the N-GQDs in THF due to solvent effect, and to 28.6% by surface-passivation with PEG_{1500} molecules (conc. of 10 mg/mL) via stabilization of excitons.[17] The highly efficient PL emission possibly resulted from the strong electron-withdrawing abilities of the N atoms, which significantly altered the whole electronic structure in N-GQDs and allowed a process of intersystem crossing emission by enhanced spin-orbital coupling.[15,17,18] In addition, the abundant zigzag-edge sites were of critical importance for superior luminescence features.[24] Moreover, their high content of O-rich groups probably made an essential contribution to the high PL quantum yields.[29,30] Figure 4d compares the quantum yields for the N-GQDs having different *N*/*C* atomic ratios. The maximum quantum yield reached up to one-order magnitude of 34.5% for N-GQDs, having the lowest *N*/*C* atomic ratio of 8.3%. In contrast, only a low quantum yield of 8.6% could be acquired for the N-GQDs having a similar *N*/*C* atomic ratio in the absence of substitutional N.[18] The observed improvement

in luminescence is greatly affected by the intrinsic chemical nature. At first, the successful doping of substitutional N dopants gives rise to a more efficient PL radiative emission, as a consequence of the restoring sp^2 hybridization and their donation of delocalization electrons entering the π^* states.[1,14,17] Second, such N-GQDs had decreased density of atomic-scale defects. These defects usually acted as a strong scattering center and electron traps, and were related to the nonradiative combination of e^--h^+ pairs.[29,42] Most importantly, as shown in Figure 4d, the quantum yields of N-GQDs were in fact inverse proportional to the N/C atomic ratios. In other words, excessive N dopants could lead to PL quenching, which is crucial to their important applications in optoelectronic devices or biosensors, possibly due to the deactivated zigzag-edge sites and effective energy transfer between N dopants and graphene.[43,44]

To further understand the correlation of N dopant concentrations with photoluminescence properties, we conducted the transient PL measurements. Figure 4e shows a typical transient PL curve of N-GQDs in Figure 4a. The transient PL spectrum was well fitted to a two-exponential function, including two decay processes with lifetimes of τ_1 = 1.92 ns (48.2% radiative emission) and τ_2 = 7.56 ns (51.8% radiative emission), yielding an average PL decay time of τ = 4.84 ns. All N-GQDs show increased PL decay times of ~4.5 ns, compared with the N-free GQDs only having a lower PL decay time of 3.6 ns (Figure S10, Supporting Information). The radiative rate constant (κ_r) and nonradiative rate constant (κ_{nr}) were therefore calculated using the equations of $\kappa_r = \phi/\tau$ and $\kappa_{nr} = (1-\phi)/\tau$, respectively. Figure 4f shows the dependence of κ_r and κ_{nr} on N/C atomic ratio. The presence of N dopants dramatically increased the radiative rate constant and simultaneously decreased the nonradiative rate constant. As increasing in N/C atomic ratio, the radiative rate constant in fact slowly decreased, while the nonradiative rate constant increased accordingly. Apparently, excessive foreign atoms of N dopants in fact led to the decreasing in quantum yields, generally through non-radiative transition back to the ground state particularly at less emissive zigzag-edges sites by energy and/or electron transfer,[43] in associate with strong scattering at point-defects.

As a demonstration of bandgap opening, the reproducible responses to ON–OFF light cycles belongs to versatile N-GQDs are shown in **Figure 5**, which were drop-casted on the florin doped tin oxide (FTO) substrate. Upon the irradiation, the generated e^--h^+ pairs in N-GQDs dissociated and produced photocurrent.[45] However, the N-GQDs in Figure 1 only created negligible photocurrent of several nA cm^{-2} under 365 nm UV light irradiation. The position of LUMO for N-GQDs was determined to –4.01 eV by cyclic voltammetric (CV) measurement (Figure S11, Supporting Information), which suggests their suitability for energy matching with metal oxide semiconductors, such as TiO_2. In fact, once the same amount of N-GQDs uniformly supported on electrospun anatase TiO_2 nanofibers (see TEM images and EDX spectrum in Figure S12, Supporting Information), they exported four orders of magnitude photocurrent of 11.8 μA cm^{-2} without any optimization, while the pure TiO_2 nanofibers only responded 2.4 μA cm^{-2}. The remarkably increased photocurrent kept almost constant during at least 20 cycles of continuous measurements (Figure S13, Supporting Information), indicating the supported N-GQDs also

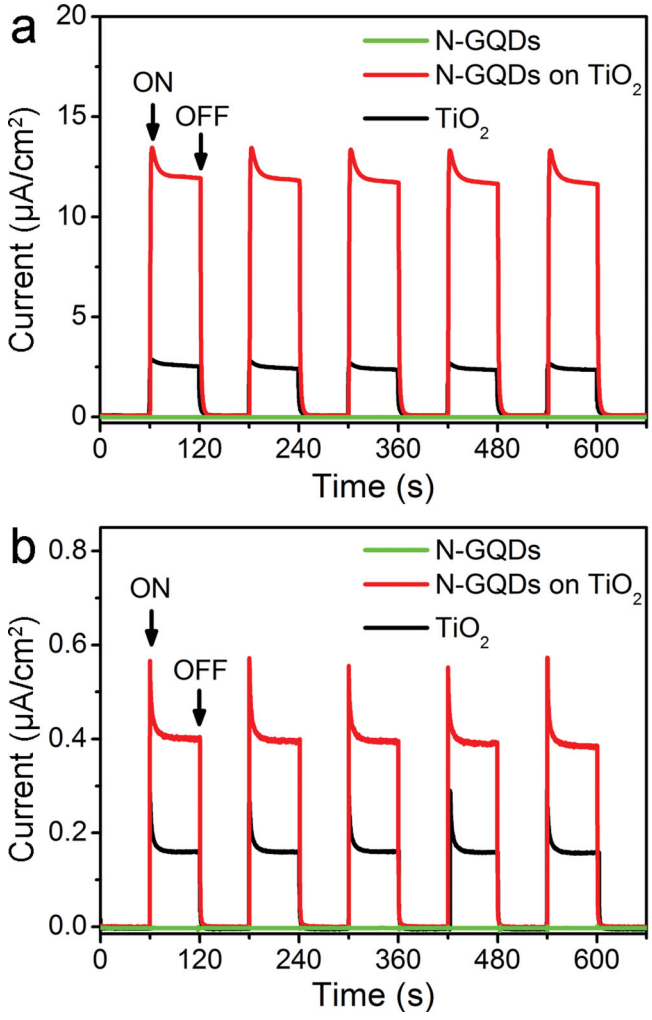

Figure 5. The reproducible ON–OFF photocurrent–time curves of N-GQDs under a) 365 nm and b) visible light (>420 nm) irradiation, exhibiting excellent abilities of photocurrent conversion.

had excellent stabilities in aqueous-contained photoelectrochemical devices. These significant improvements in terms of high photocurrent and excellent reproducibility are believed to arise from the strong interaction between N-GQDs and TiO_2, which ensured efficient e^--h^+ separation and good immobility of N-GQDs, resisting dissolution in aqueous electrolyte. The abilities of photocurrent conversation was further evidenced upon visible light (λ > 420 nm) irradiation. The supported N-GQDs had a photocurrent of 0.40 μA cm^{-2}, while the TiO_2 nanofibers only of 0.16 μA cm^{-2}. The results are not incomprehensible. Principally, it is thermodynamically favorable for the electrons injecting from LUMOs of N-GQDs to the conduction band of TiO_2, as the LUMO had a relatively higher energy than that of conduction band (–4.40 eV) for TiO_2.[46] Plus, the strong electronic couplings between N-GQDs and TiO_2 via the carboxyl-group linkers induced an ultrafast injection of electrons and restrained adverse recombination loss.[47] In this case, the TiO_2 nanofibers served as efficient 1D bridges thus facilitated the rapid transferring of electrons, boosting remarkably enhanced photocurrent.

4. Conclusions

We have demonstrated a facile approach to high concentration of N-doping in GQDs using NH_4OH as the nitrogen source via a hydrothermal method. The minimization of edge free energy resulted in their equilibrium in circular and elliptical shapes. We realized careful modulation of the *N*/*C* atomic ratios and N bonding configurations by altering the concentration of NH_4OH. The N dopants either formed pyrrolic structure or substituted the C atoms in graphene lattices, consequently allowing the N-GQDs with a significant enhancement in photoluminescence quantum yield of 34.5% without any surface passivation. The remarkable improvements were ascribed to the altered electronic structure in aromatic heterocycles by N atoms particularly at the substitutional sites, the high concentration of free zigzag sites in equilibrium shape, and their decreased defect density. Excessive N-dopants in N-GQDs in fact increased nonradiative rate constant thus led to the PL quenching, through non-radiative transition back to the ground state by energy and/or electron transfer, in associate with strong scattering at point-defects. The N-GQDs, when supported on anatase nanofibers, exhibited unique semiconducting characteristics and stable photocurrent response to UV or visible light irradiation, allowing for promising applications particularly in photovoltaic conversion devices.

Supporting Information

Supporting Information is available from the Wiley Online Library or from the author. Thirteen additional figures and one table are provided.

Acknowledgements

This work was financially supported by the National Basic Research Program (973 program, 2013CB932902), the National Natural Science Foundation of China (21201034, 21173042, 21310102005, and 51103023), the Educational Commission of Jiangsu Province (JHB2011–2), the Science and Technology Support Program (Industry) Project of Jiangsu Province (BE 2013118), and the Southeast University Innovation Fund (No. 3207042401). T.Z. acknowledges the support of the Center for Excitonics, an Energy Frontier Research Center funded by the US Department of Energy, Office of Science, Office of Basic Energy Sciences under Award Number DE-SC0001088.

Received: August 4, 2013
Revised: October 18, 2013
Published online: December 27, 2013

[1] D. Wei, Y. Liu, Y. Wang, H. Zhang, L. Huang, G. Yu, *Nano Lett.* **2009**, *9*, 1752.
[2] J. M. Englert, C. Dotzer, G. Yang, M. Schmid, C. Papp, J. M. Gottfried, H. P. Steinrück, E. Spiecker, F. Hauke, A. Hirsch, *Nat. Chem.* **2011**, *3*, 279.
[3] L. Yan, B. Zhang, F. Zhao, S. Li, X. Gao, B. Xu, P. S. Weiss, Y. Zhao, *Chem. Soc. Rev.* **2012**, *41*, 97.
[4] C. N. R. Rao, A. K. Sood, K. S. Subrahmanyam, A. Govindaraj, *Angew. Chem.* **2009**, *121*, 7890; *Angew. Chem. Int. Ed.* **2009**, *48*, 7752.
[5] L. Jiao, X. Wang, G. Diankov, H. Wang, H. Dai, *Nat. Nanotech.* **2010**, *5*, 321.
[6] D. B. Shinde, V. K. Pillai, *Angew. Chem.* **2013**, *125*, 2542; *Angew. Chem. Int. Ed.* **2013**, *52*, 2482.
[7] L. Li, G. Wu, G. Yang, J. Peng, J. Zhao, J. Zhu, *Nanoscale* **2013**, *5*, 4015.
[8] W. Liu, X. Yan, J. Chen, Y. Feng, Q. Xue, *Nanoscale* **2013**, *5*, 6053.
[9] J. Shen, Y. Zhu, X. Yang, C. Li, *Chem. Commun.* **2012**, *31*, 3686.
[10] D. B. Shinde, V. K. Pillai, *Chem. Eur. J.* **2012**, *18*, 12522.
[11] J. Bai, L. Zhang, R. Liang, J. Qiu, *Chem. Eur. J.* **2013**, *19*, 3822.
[12] D. Pan, J. Zhang, Z. Li, M. Wu, *Adv. Mater.* **2010**, *22*, 734.
[13] Q. Li, S. Zhang, L. Dai, L. Li, *J. Am. Chem. Soc.* **2012**, *134*, 18932.
[14] C. Wang, Y. Zhou, L. He, T. Ng, G. Hong, Q. Wu, F. Gao, C. Lee, W. Zhang, *Nanoscale* **2013**, *5*, 600.
[15] Y. Li, Y. Zhao, H. Cheng, Y. Hu, G. Shi, L. Dai, L. Qu, *J. Am. Chem. Soc.* **2012**, *134*, 15.
[16] Q. Li, S. Zhang, L. Dai, L. Li, *J. Am. Chem. Soc.* **2012**, *134*, 18932.
[17] H. Tetsuka, R. Asahi, A. Nagoya, K. Okamoto, I. Tajima, R. Ohta, A. Okamoto, *Adv. Mater.* **2012**, *24*, 5333.
[18] M. Li, W. Wu, W. Ren, H. M. Cheng, N. Tang, W. Zhong, Y. Du, *Appl. Phys. Lett.* **2012**, *101*, 103107.
[19] Y. Dai, Y. Jing, J. Zeng, Q. Qi, C. Wang, D. Goldfeld, C. Xu, Y. Zheng, Y. Sun, *J. Mater. Chem.* **2011**, *21*, 18174.
[20] J. Shen, Y. Zhu, C. Chen, X. Yang, C. Li, *Chem. Commun.* **2011**, *47*, 2580.
[21] Y. Dai, C. M. Cobley, J. Zeng, Y. Sun, Y. Xia, *Nano Lett.* **2009**, *9*, 2455.
[22] Y. Dai, B. Lim, Y. Yang, C. M. Cobley, W. Li, E. C. Cho, B. Grayson, P. T. Fanson, C. T. Campbell, Y. Sun, Y. Xia, *Angew. Chem.* **2010**, *124*, 10848; *Angew. Chem. Int. Ed.* **2010**, *49*, 8165.
[23] D. Pan, J. Zhang, Z. Li, M. Wu, *Adv. Mater.* **2010**, *22*, 734.
[24] J. Peng, W. Gao, B. K. Gupta, Z. Liu, R. Romero-Aburto, L. Ge, L. Song, L. B. Alemany, X. Zhan, G. Gao, S. A. Vithayathil, B. A. Kaipparettu, A. A. Marti, T. Hayashi, J. J. Zhu, P. M. Ajayan, *Nano Lett.* **2012**, *12*, 844.
[25] S. Kim, S. W. Hwang, M. K. Kim, D. Y. Shin, D. H. Shin, C. O. Kim, S. B. Yang, J. H. Park, E. Hwang, S. H. Choi, G. Ko, S. Sim, C. Sone, H. J. Choi, S. Bae, B. H. Hong, *ACS Nano* **2012**, *6*, 8203.
[26] T. Xu, K. Yin, X. Xie, L. He, B. Wang, L. Sun, *Small* **2012**, *8*, 3422.
[27] X. Jia, M. Hofmann, V. Meunier, B. G. Sumpter, J. Campos-Delgado, J. M. Romo-Herrera, H. Son, Y. Hsieh, A. Reina, J. Kong, M. Terrones, M. S. Dresselhaus, *Science* **2009**, *323*, 1701.
[28] Z. X. Gan, S. J. Xiong, X. L. Wu, C. Y. He, J. C. Shen, P. K. Chu, *Nano Lett.* **2011**, *11*, 3951.
[29] G. Eda, Y. Y. Lin, C. Mattevi, H. Yamaguchi, H. A. Chen, I. S. Chen, C. W. Chen, M. Chhowalla, *Adv. Mater.* **2010**, *22*, 505.
[30] L. L. Li, J. Ji, R. Fei, C. Z. Wang, Q. Lu, J. R. Zhang, L. P. Jiang, J. J. Zhu, *Adv. Funct. Mater.* **2012**, *22*, 2971.
[31] Y. Shao, S. Zhang, M. H. Engelhard, G. Li, G. Shao, Y. Wang, J. Liu, I. A. Aksay, Y. Lin, *J. Mater. Chem.* **2010**, *20*, 7491.
[32] J. O. Hwang, J. S. Park, D. S. Choi, J. Y. Kim, S. H. Lee, K. E. Lee, Y. H. Kim, M. H. Song, S. Yoo, S. O. Kim, *ACS Nano* **2011**, *6*, 159.
[33] K. N. Kudin, B. Ozbas, H. C. Schniepp, R. K. Prud'homme, I. A. Aksay, R. Car, *Nano Lett.* **2008**, *8*, 36.
[34] C. Gómez-Navarro, R. T. Weitz, A. M. Bittner, M. Scolari, A. Mews, M. Burghard, K. Kern, *Nano Lett.* **2007**, *7*, 3499.
[35] V. Gupta, N. Chaudhary, R. Srivastava, G. D. Sharma, R. Bhardwaj, S. Chand, *J. Am. Chem. Soc.* **2011**, *133*, 9960.
[36] C. He, S. P. Jiang, P. K. Shen, *Sci. Rep.* **2013**, *3*, 2144.
[37] X. Dong, D. Fu, W. Fang, Y. Shi, P. Chen, L. Li, *Small* **2009**, *12*, 1422.
[38] A. Lherbier, X. Blase, Y. Niquet, F. Triozon, S. Roche, *Phy. Rev. Lett.* **2008**, *101*, 036808.
[39] C. Chien, S. Li, W. Lai, Y. Yeh, H. Chen, I. Chen, L. Chen, K. Chen, T. Nemoto, S. Isoda, M. Chen, T. Fujita, G. Eda, H. Yamaguchi, M. Chhowalla, C. Chen, *Angew. Chem.* **2012**, *124*, 6766; *Angew. Chem. Int. Ed.* **2012**, *51*, 6662.

[40] J. Lu, P. S. E. Yeo, C. K. Gan, P. Wu, K. P. Loh, *Nat. Nanotechnol.* **2011**, *6*, 247.
[41] S. Kim, D. H. Shin, C. O. Kim, S. S. Kang, J. M. Kim, S. H. Choi, L. H. Jin, Y. H. Cho, S. W. Hwang, C. Sone, *Appl. Phys. Lett.* **2012**, *101*, 163103.
[42] S. Zhu, J. Zhang, X. Liu, B. Li, X. Wang, S. Tang, Q. Meng, Y. Li, C. Shi, R. Hu, B. Yang, *RSC Adv.* **2012**, *2*, 2717.
[43] M. Li, N. Tang, W. Ren, H. Cheng, W. Wu, W. Zhong, Y. Du, *Appl. Phys. Lett.* **2012**, *100*, 233112.
[44] F. Schedin, A. K. Geim, S. V. Morozov, E. W. Hill, P. Blake, M. I. Katsnelson, K. S. Novoselov, *Nat. Mater.* **2007**, *6*, 652.
[45] J. Shen, Y. Zhu, X. Yang, J. Zong, J. Zhang, C. Li, *New J. Chem.* **2012**, *36*, 97.
[46] Z. Xiong, L. L. Zhang, J. Ma, X. S. Zhao, *Chem. Commun.* **2010**, *46*, 6099.
[47] R. Long, N. J. English, O. V. Prezhdo, *J. Am. Chem. Soc.* **2012**, *134*, 14238.